Research in Astronomy and Astrophysics, 24:085007 (10pp), 2024 August https://doi.org/10.1088/1674-4527/ad5b34

A Comprehensive Classification and Analysis of Geomagnetic Storms Over Solar Cycle 24

Raja Adibah Raja Halim Shah[1], Nurul Shazana Abdul Hamid[1,2], Mardina Abdullah[2,3], Adlyka Annuar[1], Idahwati Sarudin[4], Zahira Mohd Radzi[5], and Akimasa Yoshikawa[6]
[1] Department of Applied Physics, Faculty of Science and Technology, Universiti Kebangsaan Malaysia, 43600 Bangi, Malaysia; zana@ukm.edu.my
[2] Space Science Centre (ANGKASA), Institute of Climate Change, Universiti Kebangsaan Malaysia, 43600 Bangi, Malaysia
[3] Department of Electrical, Electronic and Systems Engineering, Faculty of Engineering and Built Environment, Universiti Kebangsaan Malaysia, 43600 Bangi, Malaysia
[4] School of Physics, Universiti Sains Malaysia, 11800 USM, Pulau Pinang, Malaysia; idahwati@usm.my
[5] Malaysian Space Agency (MYSA), Kuala Lumpur, 50480, Malaysia
[6] International Research Center for Space and Planetary Environmental Science (i-SPES), Kyushu University, 819-0395 Fukuoka, Japan
Received 2024 March 12; revised 2024 May 28; accepted 2024 June 14; published 2024 July 24

Abstract

A geomagnetic storm is a global disturbance of Earth's magnetosphere, occurring as a result of the interaction with magnetic plasma ejected from the Sun. Despite considerable research, a comprehensive classification of storms for a complete solar cycle has not yet been fully developed, as most previous studies have been limited to specific storm types. This study, therefore, attempted to present complete statistics for solar cycle 24, detailing the occurrence of geomagnetic storm events and classifying them by type of intensity (moderate, intense, and severe), type of complete interval (normal or complex), duration of the recovery phase (rapid or long), and the number of steps in the storm's development. The analysis was applied to data from ground-based magnetometers, which measured the Dst index as provided by the World Data Center for Geomagnetism, Kyoto, Japan. This study identified 211 storm events, comprising moderate (177 events), intense (33 events), and severe (1 event) types. About 36% of ICMEs and 23% of CIRs are found to be geoeffective, which caused geomagnetic storms. Up to four-step development of geomagnetic storms was exhibited during the main phase for this solar cycle. Analysis showed the geomagnetic storms developed one or more steps in the main phase, which were probably related to the driver that triggered the geomagnetic storms. A case study was additionally conducted to observe the variations of the ionospheric disturbance dynamo (Ddyn) phenomenon that resulted from the geomagnetic storm event of 2015 July 13. The attenuation of the Ddyn in the equatorial region was analyzed using the H component of geomagnetic field data from stations in the Asian sector (Malaysia and India). The variations in the Ddyn signatures were observed at both stations, with the TIR station (India) showing higher intensity than the LKW station (Malaysia).

Key words: (Sun:) sunspots – Sun: activity – (Sun:) solar-terrestrial relations – Sun: coronal mass ejections (CMEs)

1. Introduction

The Sun is a variable magnetic star that exhibits changes over a wide range of timescales from mere seconds to billions of years. The Sun undergoes a natural activity cycle, known as the solar cycle, which normally completes its course in approximately 11 yr. The increase in the number of sunspots and solar flares during periods of high solar activity (SA) leads to a higher probability of coronal mass ejections (CMEs) and solar wind disturbances. An Interplanetary Coronal Mass Ejection (ICME) and Corotating Interaction Region (CIR) can be the primary drivers for geomagnetic storms when there is interaction between Earth's magnetic field and charged particles such as electrons and protons that are released from the Sun. Geomagnetic storms are defined as a temporary major disturbance that occurs when the solar wind, which contains a sudden influx of charged particles, interacts with the Earth's magnetic field, causing it to fluctuate rapidly (Gonzalez et al. 1999; Basciftci 2021). This results in a decrease in the Disturbance storm time (Dst) index, where minimum negative values indicate a stronger disturbance. The Dst index, which has been available since 1957, is a standard measurement for geomagnetic storms. The index primarily reacts to the effect of the geomagnetic field ring current (Sugiura 1963; Rostoker 1972). This Dst index is used for monitoring a geomagnetic storm's progress as it reflects the variation of its real-time intensity. Previous research indicates that occurrences driven by ICMEs are predominant during the solar maximum, while those driven by CIRs are predominant during the solar minimum and declining phases of the solar cycle (Borovsky & Denton 2006). Scientific studies of geomagnetic storms are crucial to enable the mitigation of hazards associated with space weather and technological systems, including

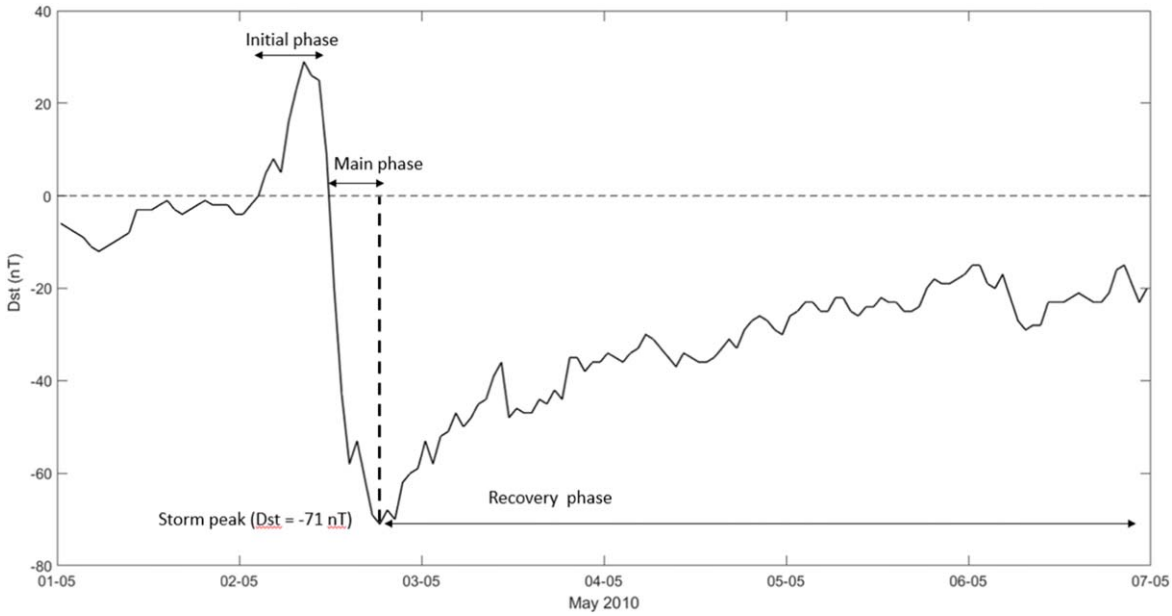

Figure 1. Illustration of geomagnetic storm phases based on Dst growth.

vulnerabilities in power grids, satellite operations, radio communications, and the integrity of metal pipelines used in oil and gas industries (Balan et al. 2016).

Previous research has mostly focused on estimating the intensity of geomagnetic storms and determining their minimum peak values. Four main categorizations of storms can be observed based on the Dst index, namely its intensity, interval, duration, and step development. Figure 1 illustrates the three distinct phases of a storm: initial, main, and recovery. The Earth's magnetosphere experiences compression when there is a sudden increment in charged particles from the solar wind approaching Earth, where this signifies the initial phase of a geomagnetic storm which usually begins with a short duration of minimum Dst peak, most often initiated by a sudden storm commencement (SSC) (Telloni et al. 2021). The main phase commences with the rapid intensification of the ring current which is driven by the energization of particle injections. During this main phase, the dynamics of Earth's magnetic field experience significant changes, and this phase typically lasts a few hours. The intensity of a geomagnetic storm is measured when the Dst values descend to a minimal value, indicating the end of the main phase and the beginning of the recovery phase. During the main phase of a geomagnetic storm, several mechanisms play a crucial role including solar wind interactions, compression of the magnetosphere, magnetic reconnection, energy transfer, particle acceleration, auroral activities, and magnetic field disturbances.

Review of past literature revealed that geomagnetic storms were observed to frequently develop in two-steps during the main phase (Kamide et al. 1998; Ghag et al. 2024). Geomagnetic storms that exhibit a two-step development show a two-step buildup in the ring current and a corresponding two-step Dst peak during their main phase. During this main phase, the strength of the Earth's magnetic field is noticeably reduced, a phenomenon which is caused by an increase in the number of particles in the magnetosphere. The recovery phase begins when the ring current initiates its decay, a process that is a result of the merger of various energetic particle loss mechanisms, where this phase can span from tens of hours up to a week. The degradation of the ring current is attributable to various factors including interaction of the Coulomb and wave-particle processes (Raghav et al. 2018). Additionally, several factors can influence the duration of the recovery phase of a geomagnetic storm. These factors include the storm's intensity, the location of the storm's impact, the state of the Earth's magnetic field before the storm, and the space weather events that occur during or after the geomagnetic storm. During these geomagnetically active periods, the thermosphere winds produced in the auroral zone extend toward mid and low latitudes, thereby driving an ionospheric disturbance dynamo (Ddyn) (Blanc & Richmond 1980; Younas et al. 2021). The Ddyn effect caused by a geomagnetic storm can be observed using geomagnetic data (Le & Amory-Mazaudier 2005; Bulusu et al. 2020).

Determining the entire storm duration is crucial as it can impact ground infrastructure through its time-integrated effects. In addition, understanding storm categorization is also vital because of its impact on the ionosphere during geomagnetic storm events (Blagoveshchenskii 2013; Liu & Shen 2017). These considerations highlight the significance of storm

Table 1
Geomagnetic Storm Categories Based on the Range of the Dst Index

Category	Range of the Dst Index
Moderate	$-100\,\mathrm{nT} < \mathrm{Dst} \leqslant -50\,\mathrm{nT}$
Intense	$-200\,\mathrm{nT} < \mathrm{Dst} \leqslant -100\,\mathrm{nT}$
Severe	$-350\,\mathrm{nT} < \mathrm{Dst} \leqslant -200\,\mathrm{nT}$
Great	$\mathrm{Dst} \leqslant -350\,\mathrm{nT}$

categorization and underscore the motivation behind the present study which aimed to analyze the comprehensive statistics of geomagnetic response growth from 2009 to 2019 (solar cycle 24), based on Dst evolution from the initial phase, through the main phase, and onto the recovery phase. Additionally, this study attempts to investigate the ICME-driven and CIR-driven geoeffectiveness that cause geomagnetic storms with different intensities. Furthermore, this paper also presents a case study that showed the equatorial magnetic signature of the ionospheric disturbance dynamo (Ddyn) effect that resulted from the geomagnetic storm event, utilizing data from the equatorial region.

2. Materials and Methods

The occurrence of geomagnetic storms for events that happened from 2009 to 2019 was identified based on the Dst index compiled by the Data Analysis Center for Geomagnetism and Space Magnetism, Kyoto University, Japan (wdc.kugi.kyoto-u.ac.jp/wdc/Sec3.html). Geomagnetic storms with a peak Dst value equal to -50 nT or less were selected. The selected geomagnetic storms were first classified into four types: moderate, intense, severe, and great, based on the range of the Dst index intensity, as shown in Table 1. Figure 1 illustrates a complete interval, including the initial, main, and recovery phases. Each complete storm interval was analyzed to separate the normal intervals from the complex events. In this study, a complex interval refers to a non-smooth interval, characterized by many noise peaks in the main phase. Additionally, a multi-storm is also considered as a complex storm when there is a continuous interval following the end of the recovery phase from the previous storm. Veselovsky & Lukashenko (2013) categorized a geomagnetic storm as complex when one event exhibits an isolated decrease in Dst and a superposition of several storms occurs, particularly when the next storm arrives before the previous storm has fully recovered. In contrast, a normal interval shows a clear variation in each storm phase without any complex disturbance or multi-storms. Examples of normal and complex intervals are provided in the Results and Discussion (Figure 5). Additionally, each interval in this study was also categorized into rapid recovery or long recovery. The duration for a rapid recovery phase must be less than 5 days; otherwise, it would be categorized under long recovery (Telloni et al. 2021). In our analysis, recovery phase was considered to have ended when the Dst value rose above -10 nT (Partamies et al. 2013; Blagoveshchensky et al. 2018).

The storm steps were further classified into step development numbers: one-step, two-step, three-step, and four-step, during the main phase as the Dst reached its minimum value (Vieira et al. 2001). One-step storms represent the normal sequence of geomagnetic storm phases, comprising an initial phase, a main phase with one single peak in the Dst value, and a recovery phase. Two-step storms exhibit a double peak decrease in their Dst value during the main phase. Accordingly, three-step and four-step storms are characterized by a decrease in the Dst value by three and four steps, respectively. Figure 2(a) depicts each phase of a geomagnetic storm with a one-step decrease in the Dst value during the main phase. Otherwise, Figure 2(b) shows a multiple peak case with a two-step storms during the main phase, which ended at the minimum Dst value. In instances where multiple negative dips occur during the main phase, these dips are counted as step numbers, identified as the second, third, and so on. When there are subsequent decreases in the Dst index following the peak value, but the peak is more positive than before, these occurrences are not counted as storms but rather as part of the recovery phase. The condition for identifying one step from another is that the duration between them must be at least 3 hr (Kamide et al. 1998). A summary of the geomagnetic storm categorization is presented in Figure 3, illustrated in the form of a flow chart.

Data from OMNI Web Data were used to obtain the value of planetary K index (Kp), component z of the interplanetary magnetic field, and solar wind speed. Identification of a CME was based on the data acquired from the SOHO LASCO CME catalog (Gopalswamy et al. 2010). ICMEs were identified using the Richardson and Cane catalog (Richardson & Cane 2010) and Wind ICME catalog (Nieves-Chinchilla et al. 2018). CIRs were identified based on three main steps in which the solar wind speed $\mathrm{Vsw} > 500\,\mathrm{km\,s^{-1}}$ (potential HSSs), exploring the solar coronal image with wavelength of 193 Å and observing the enhanced ram-pressure [Psw], density [Nsw], and IMF magnitude [B0]. More details on the CIR event identification can also be found in Hajra & Sunny (2022). The current system in the ionosphere such as the ionospheric disturbance dynamo (Ddyn) can be affected by solar wind disturbances during geomagnetic storm events. The expression of the ionospheric disturbance dynamo (Ddyn) is represented as follows (Le & Amory-Mazaudier 2005; Bulusu et al. 2020)

$$\mathrm{Ddyn} = \mathrm{H} - \mathrm{S}_R - \mathrm{EDst}, \quad (1)$$

where H is the observed component of the geomagnetic field during the storm period, and S_R is H component of the geomagnetic field during the nearest quiet day. Meanwhile, EDst is mean nighttime H component value variations observed at MAGDAS stations along the magnetic equatorial region (Uozumi et al. 2008; Hamid et al. 2013).

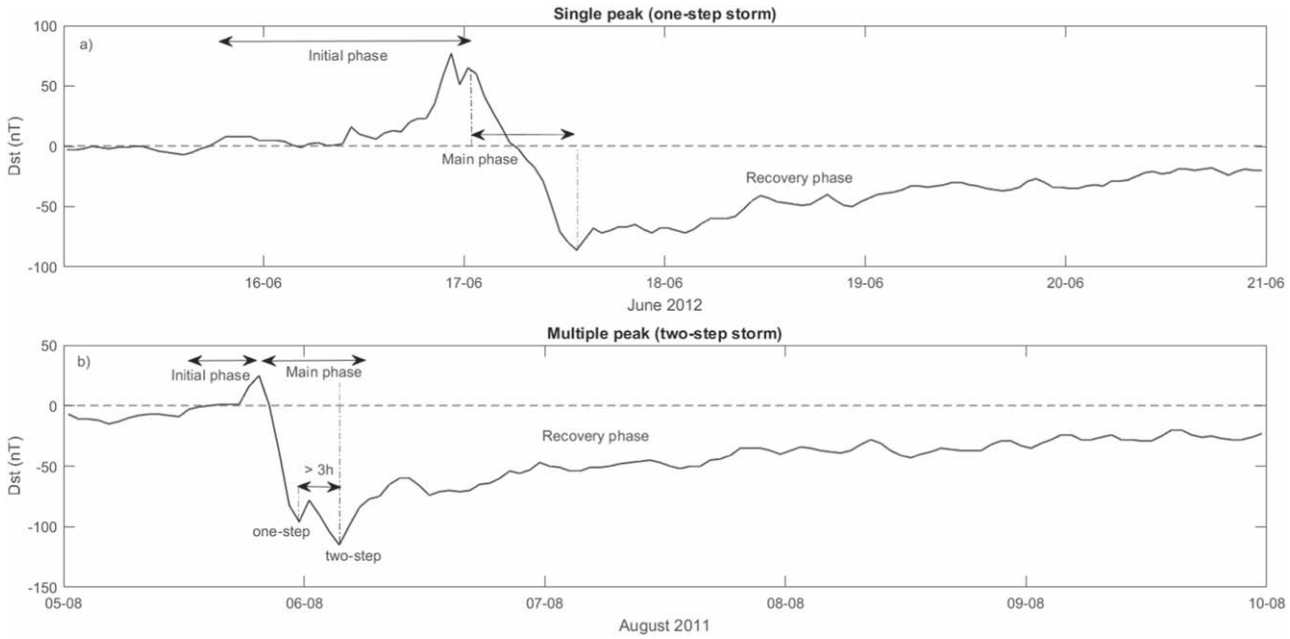

Figure 2. Geomagnetic storm phases with (a) single peak storm (one-step development) and (b) multiple peak storm (two-step development).

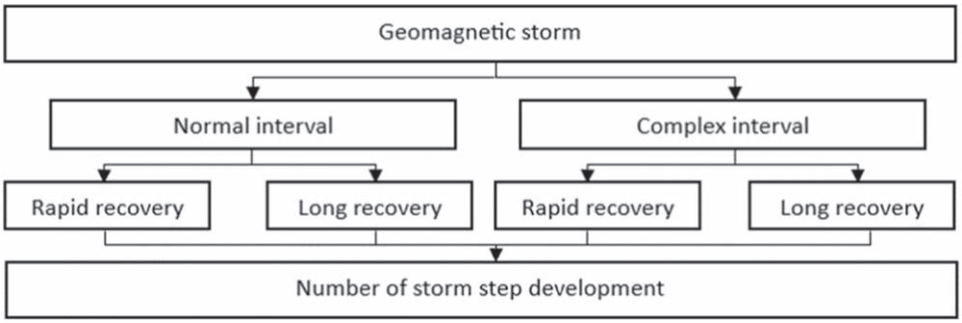

Figure 3. Flow chart of geomagnetic storm categorization.

3. Results and Discussion

3.1. Distribution and Categorization of Geomagnetic Storms During Solar Cycle 24

Figure 4 shows the distribution of all geomagnetic storms during solar cycle 24, which comprised moderate, intense, and severe storms, along with the corresponding sunspot numbers. The total number of geomagnetic storms for the period of 2009–2019 was 211 storms, which included 177 moderate storms (84%), 33 intense storms (15%), and 1 severe storm (1%), with no great storm (0%) recorded. Overall, the statistics of geomagnetic storms showed the occurrences of storms with moderate type appeared to be dominant over the years. The division of the SA level depends on the sunspot numbers. Statistics presented in Figure 4 affirm that there was less storm activity, with only moderate storms during the beginning and end of the low SA levels for solar cycle 24, specifically in 2009–2010 and 2018–2019. Meanwhile, during periods of high SA levels (2011–2014), a higher number of storm activities was observed compared to periods of low SA levels, and this included the observation of one severe storm in 2015.

Based on Figure 4, it can be observed that the occurrences of geomagnetic storms are closely related to the variations of sunspot numbers. In this solar cycle, the dual peak variation of sunspots was observed in 2011 and 2014, where both peaks of the geomagnetic storm occurrences were observed to be a year after the highest value of SA, which was in 2012 and 2015. In their study, Le et al. (2013) found the occurrence of geomagnetic storms increased as the sunspot numbers increased, and geomagnetic storms peaked two or three years after the peak of SA (sunspots). This inconsistency of peak year between sunspot numbers and storm occurrence during the

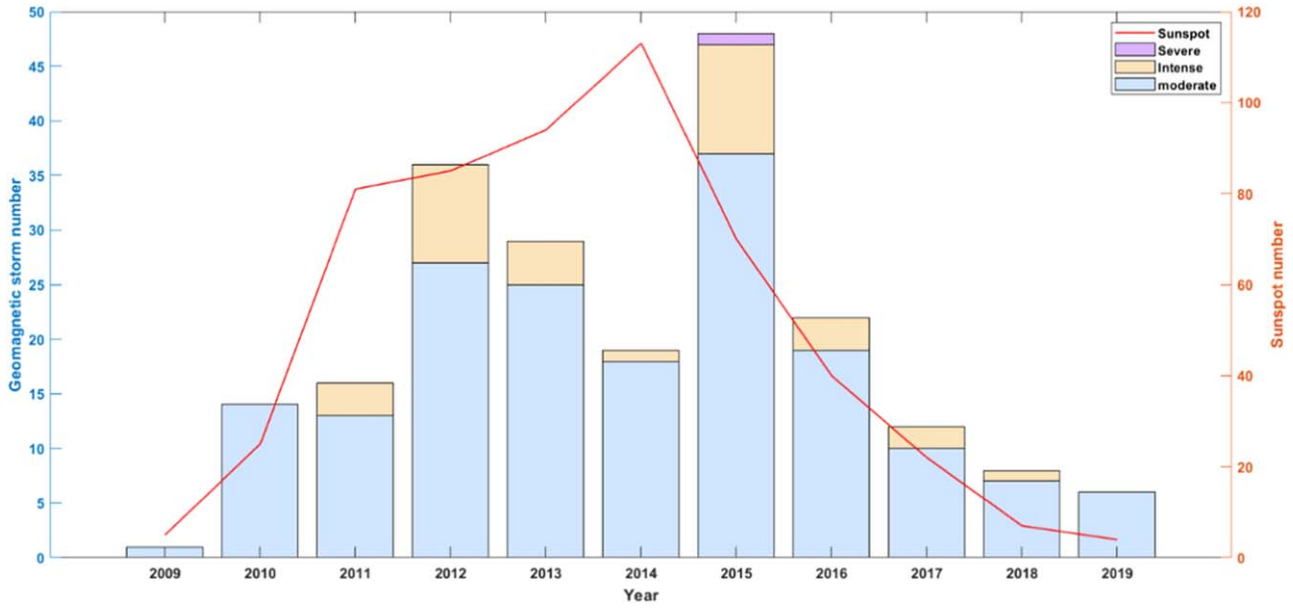

Figure 4. Number of geomagnetic storms based on their storm type along with the sunspot numbers for solar cycle 24 (2009–2019).

latest complete data of solar cycle 24 aligns with the findings of a previous study that used data from solar cycle 23. The study by Echer et al. (2011) also reported that two peaks of geomagnetic storms were observed during solar cycle 23, where the first peak occurred around solar maximum and the second peak during the beginning of the declining phase. In solar cycle 24, about 36% and 23% of geomagnetic storms are found to occur due to the ICMEs (ICME-driver) and CIRs (CIR-driver), respectively. When categorized by storm type, 25% of ICMEs and 21% of CIRs resulted in moderate storms, while 10% of ICMEs and 1% of CIRs caused intense storms, with only 1% of ICMEs leading to severe storms. Most of the hypotheses in previous studies stated that the stronger storms during the maximum and early declining phase were caused by CME or large active region activity (Gonzalez et al. 2007; Echer et al. 2008). In contrast, weaker storms during the declining phase were reported to be contributed by CIR activity. It is apparent that more than half of the moderate storms are impacted by both CME and ICME drivers, with minimal disparity between the two. Nevertheless, a noteworthy observation indicates that the majority of intense storms are primarily caused by ICME drivers when compared to the CIR drivers. Additionally, in previous study during the solar cycle 23, statistics show that 22% of CIRs were geoeffective and caused moderate storms, while 2.5% of CIRs resulted in intense storms (Chi et al. 2018).

Figure 5 presents examples of the general profile for a complete geomagnetic storm interval which consists of the initial phase, the main phase (including the step number), and the recovery phase. Figure 5(a) shows a clear one-step storm (2015 January 7) which had a minimum Dst of -107 nT and was categorized as an intense storm, with a long recovery phase that lasted $\sim$10 days. In contrast, the storm (2016 January 1) displayed in Figure 5(b) was characterized by the Dst index as a two-step storms where the first step showed a Dst of -58 nT (moderate storm), and the second step showed a Dst of -116 nT (intense storm), with a rapid recovery phase that only lasted $\sim$4 days. Figure 5(c) presents a more complex storm (2015 September 9), with three-step storms. The first and second steps were classified as moderate storms, with Dst values of -50 nT and -75 nT, respectively. The third step with the minimum Dst value of -105 nT, exceeded the intense storm threshold, and its had a long recovery phase that ended after $\sim$10 days. Figure 5(d) depicts a similar storm situation with four-step storms (2015 August 27) that had a rapid recovery which ended after $\sim$3 days. The first three storm steps were of moderate type with Dst values of -57 nT, -79 nT, -92 nT, respectively, and the fourth step was of intense type with a Dst value of -103 nT. According to Richardson & Zhang (2008), the number of storm steps is not necessarily directly related to the number of interplanetary activities involved during the storm's growth. Based on this example of storm categorization, the statistics of all storm occurrences during solar cycle 24 are presented in Figure 6.

Figure 6(a) displays the variations in the number of geomagnetic storm steps along with the sunspot numbers from 2009 to 2019. Concerning the number of storm steps in solar cycle 24, it was found that 79 intervals featured a one-step storm, 48 intervals had two-step storms, 8 intervals experienced three-step storms, and 3 intervals exhibited four-step storms.

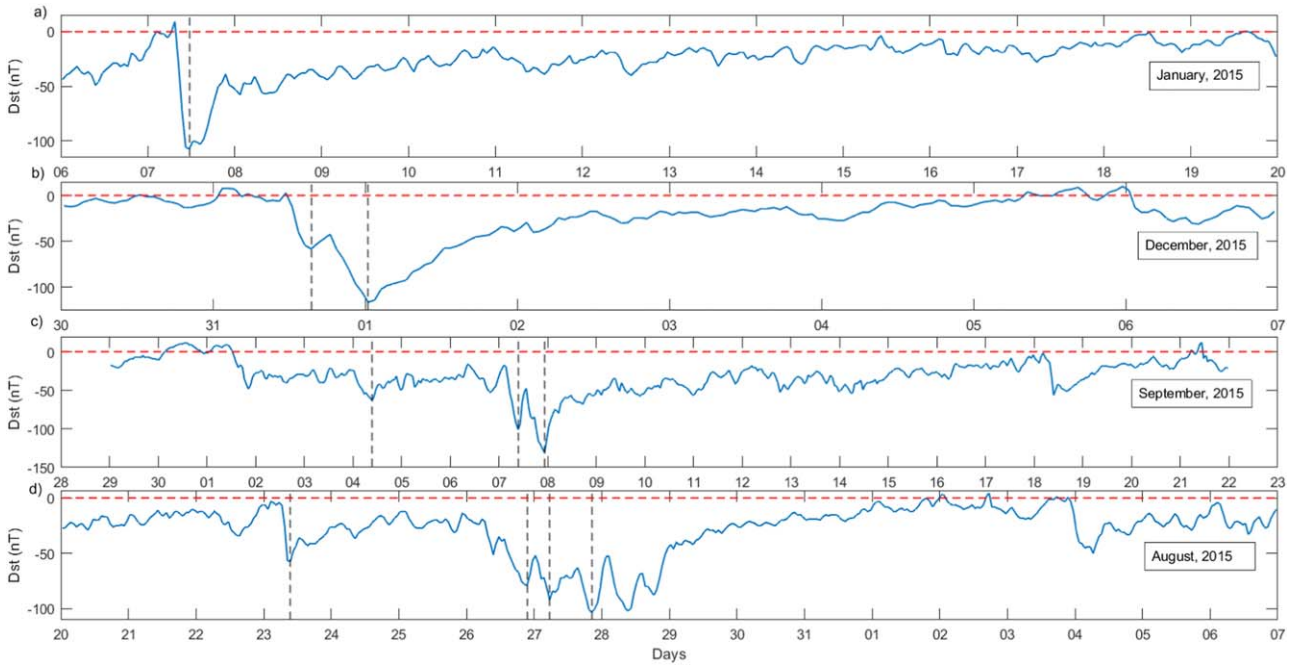

Figure 5. Examples of geomagnetic storms with (a) normal interval, one-step storm, long recovery; (b) normal interval, two-step storms, rapid recovery; (c) complex interval, three-step storms, long recovery; (d) complex interval, four-step storms, rapid recovery. The storm steps are represented in black dashed lines.

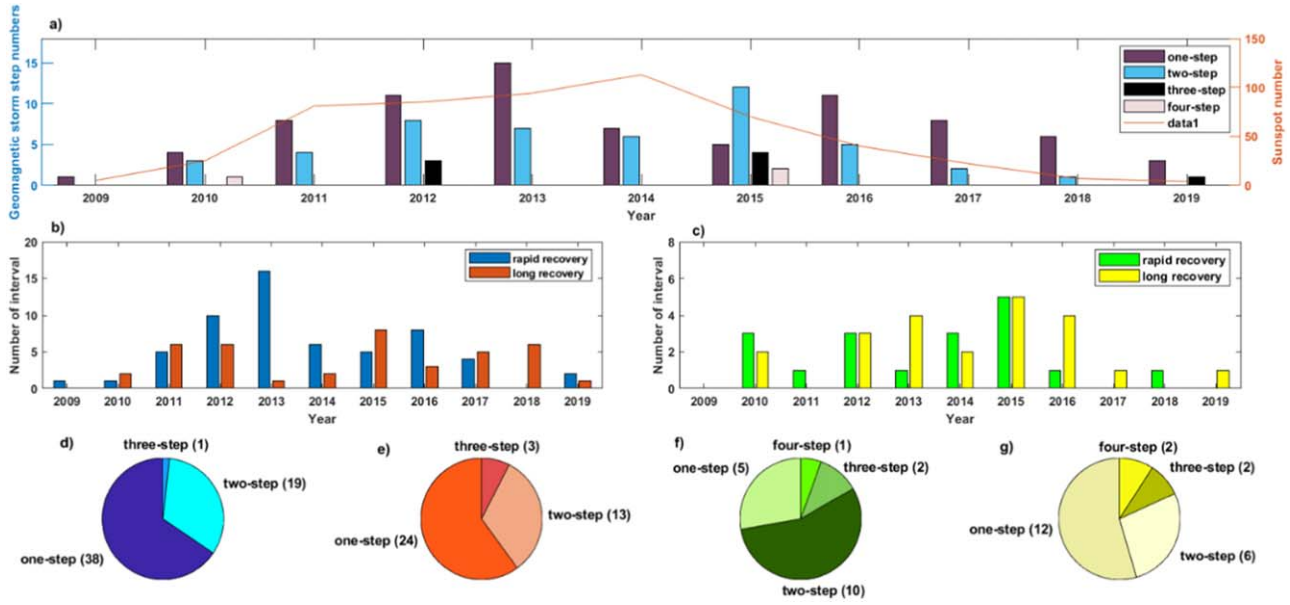

Figure 6. The total number of steps along with the sunspot number from 2009 to 2019. Number of geomagnetic storms (b) with normal intervals and (c) complex intervals that have rapid and long recovery phases from 2009 to 2019. Number of storm steps in normal intervals (d) with rapid recovery and (e) with long recovery. Number of storm steps in complex intervals (f) with rapid recovery and (g) with long recovery.

The analysis revealed that, throughout the year, one-step storm predominated, accounting for 57% of the total, followed by two-step storms which constituted 35%. Previous studies by Kamide et al. (1998) and Richardson & Zhang (2008) found 29% and 59% of storms, respectively, were predominantly classified as one-step storm, and these storms were limited to a single storm type, which was intense ($-200\,\mathrm{nT} < \mathrm{Dst} \leqslant -100\,\mathrm{nT}$). Additionally, Kamide et al. (1998) also analyzed all

storm types and found that 40% were categorized as one-step storm and 53% as two-step storms, with their data covering approximately three previous solar cycles. Meanwhile, in this current study, approximately 6% of the storms observed in 2012, 2015 and 2019 were classified as three-step storms, and the remaining 2% of storms were identified as four-step storms, which were observed in 2010 and 2015. Notably, all step numbers were also found to occur in 2015 as it was also the peak year for geomagnetic storm occurrences in this current complete solar cycle 24. Veselovsky & Lukashenko (2013), who conducted an analysis on solar cycle 23, also found that the contribution of storm events with multiple steps was larger during the maximum and the declining phases of the solar cycle.

In the case of single peak storms, 89% exhibit moderate storms, while 11% display intense storms. Conversely, multiple peak storms typically manifest in two or more steps, comprising 79% moderate, 27% intense, and 2% severe. Vieira et al. (2001) observed that 28% of intense storms exhibited a one-step pattern in the previous solar cycle. Additionally, research by Kamide et al. (1998) covering solar cycles 20, 21, and 22 found that 50% of intense storms displayed a two-step pattern. This shows a higher percentage of intense storms with multiple steps when compared to the current solar cycle. Furthermore, within the normal interval, 63% are classified as moderate storms, 18% as intense storms, and a mere 1% as severe storms. Conversely, within the complex interval, 89% are identified as moderate storms and 11% as intense storms. It is evident that moderate storms predominate at both types of intervals.

Complex storms with multiple steps usually occur during the maximum phase due to the superimposition of SAs during periods of disturbance. This observation aligns with solar cycle 24, where the analysis revealed that during the maximum and declining phases, multiple numbers of steps were observed with instances of up to four-step storms in one complete interval of a geomagnetic storm. Analysis indicates that 43% and 42% of single peak storms are attributable to ICME and CIR drivers, respectively. Conversely, for multiple peak storms, 57% are influenced by ICME drivers, while 58% are driven by CIR. Notably, both drivers demonstrate a comparable contribution to the occurrence of single peak and multiple peak storms, with no significant difference observed. On the other hand, storms driven by CIRs demonstrate a 52% normal interval and a 48% complex interval. In contrast, storms caused by ICMEs exhibit a 73% normal interval and a 27% complex interval.

The presentation of the results next proceeds with an analysis of the storm statistics based on normal and complex intervals, which are both presented in Figure 6(b) and (c), respectively. Throughout both types of intervals, no discernible significant trend or variation in the number of geomagnetic storms was observed over the years, for both rapid recovery and long recovery phases, across the entirety of solar cycle 24. Over the course of the 11 yr of the solar cycle, there were 98 normal intervals, of which 58 intervals displayed rapid recovery and 40 intervals exhibited long recovery phases. In contrast, among the 40 complex intervals identified, 18 intervals exhibited rapid recovery while 22 intervals showed long recovery phases. In light of this analysis, it was evident that most storms with complex intervals showed a prolonged recovery phase. According to Veselovsky & Lukashenko (2013), this prolonged recovery phase can be attributed to multiple factors, including several small magnetic clouds, numerous solar flare eruptions, CMEs, and filaments passing along Earth's orbits during the next solar rotation. The analysis indicates that storms exhibiting rapid recovery are attributed 60% to ICME drivers, while 46% are associated with CIR drivers. Conversely, storms characterized by a long recovery phase are attributed to ICME and CIR drivers in 40% and 54% of cases, respectively. Study by Matamba & Habarulema (2018) found that a storm being CIR-driven had a longer recovery period compared to a storm being ICME-driven. Statistics reveal that 47% of storms exhibit a moderate type and 7% demonstrate an intense type, undergoing a rapid recovery phase. In contrast, 36% of storms manifest a moderate type, 9% have an intense type, and 1% have a severe type, experiencing a long recovery phase.

Single and multiple interplanetary disturbances that are capable of causing complex geomagnetic storms may originate from the Sun, and these disturbances can arise from the same or different areas of active regions, depending on several conditions (Veselovsky & Lukashenko 2013). For normal intervals, the step development was observed to show up to three-steps, with 3 intervals of three-step storms observed with long recovery phase. In Figure 6(d), a total of 58 intervals was categorized as normal intervals with rapid recovery phases. These include 38 intervals exhibiting one-step storm, 19 intervals with two-step storms, and a single interval featuring three-step storms. In contrast, Figure 6(e) shows 40 normal intervals with long recovery phases, comprising a compilation of 24 intervals with one-step storm, 13 intervals with two-step storms, and 3 interval with three-step storms. Meanwhile, for complex intervals, observations revealed storms of up to four-steps. Figure 6(f) presents 18 complex intervals with rapid recovery phases, comprising a combination of 5 intervals with one-step storm, 10 intervals with two-step storms, 2 intervals with three-step storms and 1 interval with four-step storms. Additionally, Figure 6(g) shows a total of 22 complex intervals with long recovery phases which can be clustered into 12 intervals with one-step storm, 6 intervals with two-step storms, 2 intervals with three-step storms, and 2 intervals with four-step storms. Notably, it was only in 2015, the year that marked the peak of geomagnetic storm occurrences, that a variety of step numbers could be observed. Step development reached up to four-step storms during this time.

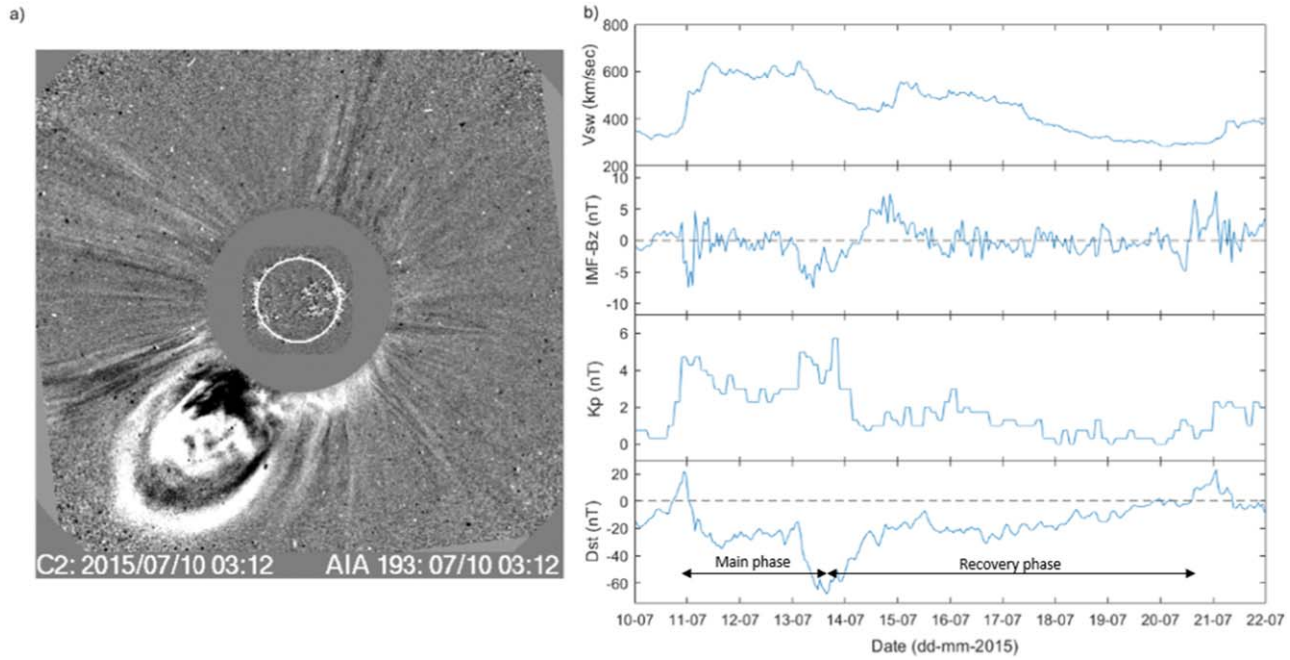

Figure 7. (a) The coronagraphic image of a CME on 2015 July 10. (b) The solar wind speed (Vsw), component z of the interplanetary magnetic field, IMF, Kp index, and Dst index from 2015 July 10 to July 21.

In summary, most of the previous studies on geomagnetic storms have mainly focused on the average characteristics of a single storm event, where these studies generally assume a smooth, single storm at the main phase followed by a slow and relatively steady increase in the Dst value during the recovery phase. However, the analysis in this present study revealed that many cases of geomagnetic storms were followed by multiple decreases in Dst before fully recovering to pre-storm levels. Kamide et al. (1998) in their study found that most intense storms were followed by a two-step development of geomagnetic storms. Other past studies also identified geomagnetic storms with three-step development during the main phase (Chukwuma 2010; Olabode & Ariyibi 2020). Additionally, Vieira et al. (2001) found that 20% of intense storms, out of 49 selected events, had three or more steps that were driven by magnetic clouds. This step development of geomagnetic storms in the ring current can culminate in an intense storm due to the superposition of two successive moderate storms.

3.2. Case Study of the Impact of Geomagnetic Storms on Ddyn

A geomagnetic storm event is a space weather phenomenon that mainly occurs in the Earth's environment. This event is mainly triggered by space weather activities that occur on the Sun's surface, such as CME. In general, the storm can produce a significant impact on the Earth's ionosphere, which is primarily due to plasma ejection (Hamid et al. 2023). For this reason, further analysis was conducted through a case study to observe the contribution of CME to geomagnetic storm events and their subsequent influence on the electric current in the ionosphere with the presence of Ddyn. The partial halo CME, on 2015 July 10, was selected as it is related to the geomagnetic storm event that occurred on 2015 July 13. Figure 7(a) shows the coronagraphic image of the partial halo CME on 2015 July 10, (03:12 UT), which is a type of CME that is seen as a partial circular halo around the Sun when it is viewed from Earth.

Figure 7(b) illustrates the variations in solar wind speed (Vsw), IMF-Bz, Kp index, and Dst index from 2015 July 10 to July 21. The solar wind showed a sudden increase in speed from $\sim$300 km s^{-1} to $\sim$600 km s^{-1} on 2015 July 11, indicating the onset of the solar wind's entry into the Earth's magnetosphere. Concurrently, as the pressure increased due to the CME, the Bz turned southward, reaching ~-8 nT, where this southward orientation of the interplanetary magnetic field indicated an enhanced interaction between the solar wind and Earth's magnetosphere. The duration of the geomagnetic storm's main phase can be described by the length of time or duration the Bz component remains negative (Tang et al. 1989; Ghag et al. 2024). An earlier study revealed that as the Bz becomes more negative, the Dst value also tends to be high, indicating intense geomagnetic storms (Rathore et al. 2014; David et al. 2022). An SSC was observed in this interval,

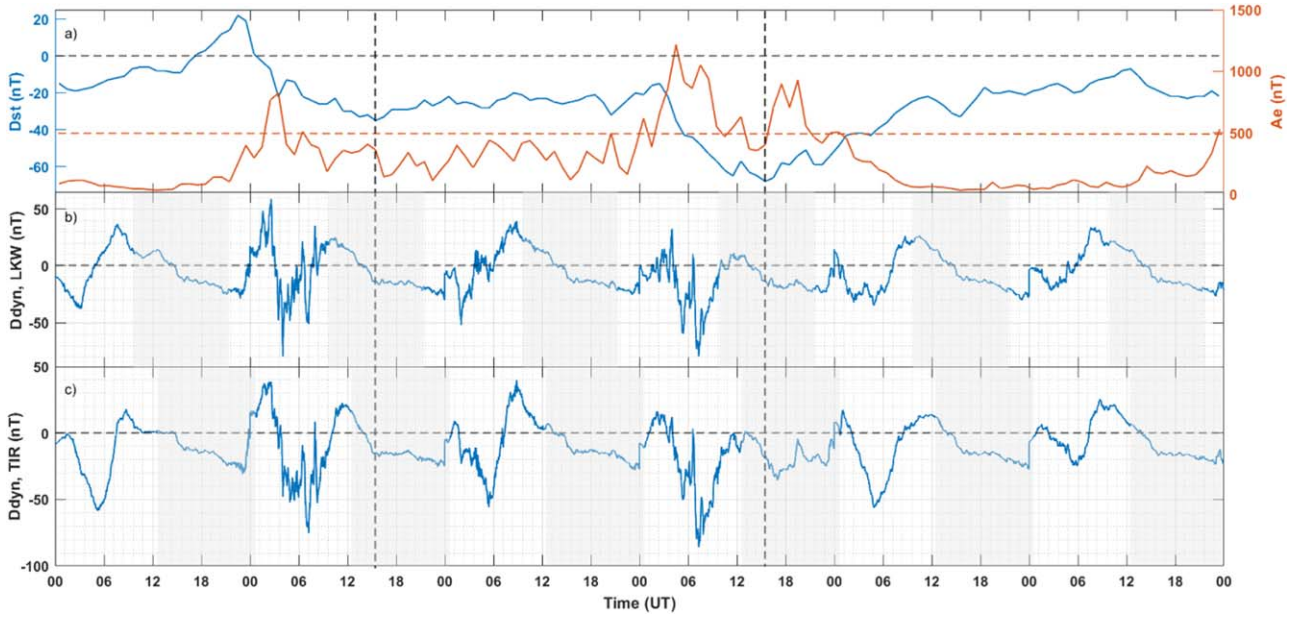

Figure 8. (a) The Dst index and AE index for geomagnetic storms occurring from 2015 July 10 to July 15, along with the variation of the Ddyn in the Asian sector for the (b) LKW station (Langkawi) and (c) TIR station (India). The shaded areas represent the nightside of the local time at each station. A vertical dashed line indicates the peak of the storm.

indicated by a Dst value of ∼20 nT, which was brought about by the enhancement in the magneto-pause current. During the same period, the Kp index reached a value of 5 during the first step of the geomagnetic storm, corresponding to a Dst value of −35 nT. Subsequently, the value of the Kp index increased to 6 during the second step of the geomagnetic storm, with a Dst value of −68 nT. As the geomagnetic storm entered the recovery phase that lasted around ∼6 days, the solar wind speed, IMF Bz, Kp, and Dst index returned to normal.

The study continued to observe the general effect in the presence of Ddyn associated with this geomagnetic storm which exhibited a one-step development as it is one of the dominant storm types in the current solar cycle. Figure 8 illustrates the variations of the Dst index, Ae index, and Ddyn in the Asian sector, as indicated by data from stations (c) LKW (Malaysia) and (d) TIR (India). Due to data availability, this study focused solely on observing the effects on this sector during this selected storm event. Figure 8(a) illustrates the variations of the Dst index and Ae index, showing a correlation between the two, whereby as the Dst index reached a minimum, the Ae index increased to a high value, confirming the disturbance in the Earth's ionosphere. The shaded part in Figure 8(b) and (c) represents the nightside of the local time at each station, while the non-shaded part represents the dayside. Within a single interval, two storms were observed, categorized as weak and moderate types The first drop in the Dst index (first vertical dashed line) occurred at 15:00 UT on 2023 July 11, reaching a value of −35 nT, indicative of a weak storm. Immediately after this event, the Ddyn at the LKW station was not significant during the local daytime, from 10:00 UT (06:00 LT) to 03:00 UT (11:00 LT). However, the presence of the southward Ddyn was clearly observed at the TIR station, with a value of ∼−40 nT, from around 02:00 UT (07:30 LT) to 07:00 UT (12:30 LT).

The Dst began to drop again and reached its minimum value on 2023 July 13, (second vertical dashed line), indicating the commencement of the second geomagnetic storm with a value of −68 nT (moderate storm) at 15:00 UT. A few hours after the peak, the auroral activity started to weaken again, falling to a value of less than 500 nT at around 23:00 UT during the recovery phase. At the LKW station, a small fluctuation that showed a southward disturbance of the Ddyn was observed, reaching a value of −20 nT from 01:00 UT (09:00 LT) to 07:00 UT (15:00 LT). Contrastingly, at the TIR station, a strong signature of the Ddyn could be clearly observed, with a value of −50 nT from 02:00 UT (07:30 LT) to 08:00 UT (13:30 LT). The observed variations in the Ddyn showed different intensity because of the differing impacts of the weak and moderate geomagnetic storm types. Additionally, the attenuation of the Ddyn can also vary across different longitudes (Le & Amory-Mazaudier 2005; Joshi & Rao 2020). However, the analysis of data from these two stations, which are both located in the same sector (Asian sector), revealed a higher value of Ddyn at the TIR station compared to the LKW station, with a notable difference of ∼30 nT.

4. Conclusion

In this study, the statistical analysis of geomagnetic storms and their classifications based on type, step development, and phases were conducted using the Dst index as a parameter. From 2009 to 2019, a total of 211 geomagnetic storms was observed, comprising 177 moderate, 33 intense, and one severe storm, with no storms categorized as great. Each identified geomagnetic storm had a complete interval which included an initial phase, a main phase, and a recovery phase. Over the span of 11 yr, there were 58 normal intervals with rapid recovery, 40 normal intervals with long recovery, 18 complex intervals with rapid recovery, and 22 complex intervals with long recovery. Additionally, the study identified 79 intervals with one-step storm, 48 intervals with two-step storms, 8 intervals with three-step storms, and 3 intervals with four-step storms during their main phases. Besides, 36% and 23% of storms are caused by ICME-driven and CIR-driven, respectively. The analysis conducted also included examination of a moderate storm that was triggered by a partial halo CME on 2015 July 10. This geomagnetic storm, which had a normal interval, exhibited a two-step development during its main phase, where the first peak Dst was ~ -35 nT (15:00 UT, 2015 July 11) and the second peak Dst was ~ -68 nT (15:00 UT, 2015 July 13), followed by a long recovery phase which lasted ~ 6 days. Corresponding to the period after the first Dst peak when the Ae < 500 nT, the Ddyn showed clear attenuation only at the TIR observatory station. However, after the second Dst peak, during weak auroral activity, the signature of Ddyn was clearly observed in both stations, with a higher value of Ddyn at the TIR station (~ -50 nT) compared to the LKW station (~ -20 nT) during the dayside of the local time.

Acknowledgments

The authors extend their gratitude for the funding by Fundamental Research Grant Scheme (FRGS) under Ministry of Higher Education (KPT) Malaysia with the grant No. FRGS/1/2023/STG07/UKM/02/1. Special thanks are extended to the Malaysian Space Agency (MYSA) and the MAGDAS Malaysia team for their contribution in the sustainability of the operation of the MAGDAS Langkawi station, Malaysia. I.S. is supported by Universiti Sains Malaysia through Short-Term Grant with project No. 304/PFIZIK/6315730. A.Y. is supported by JSPS KAKENHI grant Nos. JP20H01961, JP22K03707, JP21H04518, JP22K21345. The interplanetary parameters provided by OMNI data were obtained through the GSFC/SPDF OMNIWeb interface. The free Dst data were provided by the Data Analysis Centre for Geomagnetism and Space Magnetism (WDC Kyoto). The CME catalog is generated and maintained at the CDAW Data Center by NASA and The Catholic University of America in cooperation with the Naval Research Laboratory.

References

Basciftci, F. 2021, Ge&Ae, 61, S156
Balan, N., Batista, I. S., Tulasi, R. S., & Rajesh, P. K. 2016, GSL, 3, 3
Blanc, M., & Richmond, A. D. 1980, JGR, 85, 1669
Blagoveshchenskii, D. V. 2013, Ge&Ae, 53, 275
Bulusu, J., Archana, R. K., & Arora, K. 2020, JGRA, 125, e2019JA027718
Blagoveshchensky, D. V., Maltseva, O. A., & Sergeeva, M. A. 2018, AnGeo, 36, 1057
Borovsky, J. E., & Denton, M. H. 2006, JGRA, 111, A07S08 JGRA
Chukwuma, V. U. 2010, AcGeo, 58, 1164
Chi, Y., Shen, C., Luo, B., Wang, Y., & Xu, M. 2018, SpWea, 16, 1960
Richardson, I. G., & Cane, H. V. 2010, SoPh, 264, 189
David, T. W., Adekoya, B. J., Michael, C. M., et al. 2022, JNSPS, 4, 620
Echer, E., Gonzalez, W. D., & Tsurutani, B. T. 2011, JASTP, 73, 1454
Echer, E., Gonzalez, W. D., Tsurutani, B. T., & Gonzalez, A. L. C. 2008, JGRA, 113, A05221
Gonzalez, W. D., Tsurutani, B. T., & Clua De Gonzalez, A. L. 1999, SSRv, 88, 529
Ghag, K., Raghav, A., Bhaskar, A., et al. 2024, AdSpR, 73, 6288
Gopalswamy, N., Yashiro, S., Michalek, G., et al. 2010, SunGe, 5, 7
Gonzalez, W. D., Echer, E., Clua-Gonzalez, A. L., & Tsurutani, B. T. 2007, GeoRL, 34, L06101
Hajra, R., & Sunny, J. V. 2022, SoPh, 297, 30
Hamid, N. S. A., Halim, R. A. R., Sarudin, I., Yoshikawa, A., & Fujimoto, A. 2023, SM, 52, 2309
Hamid, N. S. A., Liu, H., Uozumi, T., & Yumoto, K. 2013, Antarct. Rec., 57, 329
Joshi, S., & Rao, K. M. 2020, JSR, 12, 233
Kamide, Y., Yokoyama, N., Gonzalez, W., et al. 1998, JGRA, 103, 6917
Le, H. M., & Amory-Mazaudier, C. 2005, JGRA, 110, A10301
Liu, G., & Shen, H. 2017, AdSpR, 59, 2301
Le, G.-M., Cai, Z.-Y., Wang, H.-N., Yin, Z.-Q., & Li, P. 2013, RAA, 13, 739
Matamba, T. M., & Habarulema, J. B. 2018, SpWea, 16, 538
Nieves-Chinchilla, T., Vourlidas, A., Raymond, J. C., et al. 2018, SoPh, 293, 31
Olabode, A. O., & Ariyibi, E. A. 2020, SciAf, 9, e00472
Partamies, N., Juusola, L., Tanskanen, E., & Kauristie, K. 2013, AnGeo, 31, 349
Rostoker, G. 1972, RvGSP, 10, 935
Raghav, A. N., Kule, A., Bhaskar, A., Mishra, W., Vichare, G., & Surve, S. 2018, ApJ, 860, 7
Rathore, B. S., Gupta, D. C., & Parashar, K. K. 2014, IJG, 05, 1602
Richardson, I. G., & Zhang, J. 2008, GeoRL, 35, 6
Sugiura, M. 1963, Hourly values for magnetic storm variation for International Geophysical Year NASA-TM-X-55238, NASA Technical Reports Server
Telloni, D., D'Amicis, R., Bruno, R., et al. 2021, ApJ, 916, 64
Tang, F., Tsurutani, B. T., Gonzalez, W. D., Akasofu, S. I., & Smith, E. J. 1989, JGR, 94, 3535
Uozumi, T., Yumoto, K., Kitamura, K., et al. 2008, EP&S, 60, 785
Veselovsky, I. S., & Lukashenko, A. T. 2013, Ge&Ae, 53, 595
Vieira, L. E. A., Gonzalez, W. D., Clua De Gonzalez, A. L., & Dal Lago, A. 2001, JASTP, 63, 457
Younas, W., Amory-Mazaudier, C., Khan, M., & Le Huy, M. 2021, SpWea, 19, 9